Heliyon 10 (2024) e30691

Contents lists available at ScienceDirect

Heliyon

journal homepage: www.cell.com/heliyon

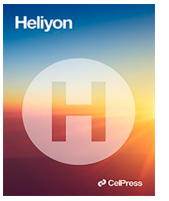

Research article

Characterization of co-fired sodium-ion conductive $Na_2Ni_2TeO_6$ and $Na_2Zn_2TeO_6$ with honeycomb layer structure

Kazuki Yamamoto, Yuki Ono, Ryoji Inada *

Department of Electrical and Electronic Information Engineering, Toyohashi University of Technology, 1-1 Hibarigaoka, Tempaku-cho, Toyohashi, Aichi, 441-8580, Japan

ARTICLE INFO

Keywords:
Honeycomb layered oxide
Co-firing
Sodium-ion conductivity
Solid-state batteries

ABSTRACT

We investigated the reactivity of P2-type honeycomb layered oxides $Na_2Ni_2TeO_6$ (NNTO) and $Na_2Zn_2TeO_6$ (NZTO) co-fired at the temperature from 500 °C to 800 °C. From X-ray diffraction measurements, it was found that the reaction between NNTO and NZTO is unremarkable at the temperature below 700 °C. However, when annealed at 800 °C, they formed the solid-solution phase without any secondary phases. The NNTO and NZTO composite pellets co-fired at 800 °C showed sodium-ion conductivity well above 10^{-4} S cm^{-1} at room temperature, indicating that the solid-solution phase of NNTO and NZTO has good ionic conductivity. A maximum room temperature conductivity of 7.4×10^{-4} S cm^{-1} was confirmed at the mixing ratio NNTO: NZTO = 0.5 : 1.5. These results can be applied to the fabrication of all-solid-state batteries using NNTO as the cathode active material and NZTO as the solid electrolyte via a simple co-sintering process.

1. Introduction

Rechargeable secondary batteries are key devices contributing to the realization of a carbon-neutral society. To expand their applications, improvements in the energy density, safety, and reliability of batteries are strongly desired [1]. All-solid-state sodium (Na) ion batteries (NiBs) are promising high-safety and low-cost alternative energy storage devices for current lithium-ion batteries, and are particularly suitable for application in large-scale energy storage systems [2–7]. The development of inorganic solid Na-ion conducting materials for use as solid electrolytes is critical for realizing all-solid-state NiBs. Solid electrolyte materials should not only have high Na-ion conductivity above 1 mS cm^{-1} at room temperature but also chemical and electrochemical stabilities against both positive and negative electrode active materials. Although oxide based solid electrolyte materials have lower conductivity and deformability than sulfide and halide-based ones, they offer advantages such as chemical stability in air and ease of handling [3–7].

$Na_2M_2TeO_6$ (NMTO, M = Zn, Mg, Ni, Co, etc.) with a P2-type honeycomb layer structure is a fast Na-ion conductive oxide [8]. In this compound, each TeO_6 octahedron is surrounded by six MO_6 octahedra via edge-sharing. Na ions are located between layers at three different sites, all of which are partially occupied; thus, they can migrate between them [8,9]. $Na_2Zn_2TeO_6$ (NZTO) is an attractive candidate as a solid electrolyte because of its high ionic conductivity well above 10^{-4} S cm^{-1} at room temperature and electrochemical stability against metallic Na [10–16]. A wide electrochemical potential window from 0 to 4 V vs. Na/Na^+ has been experimentally confirmed in previous studies on NZTO [10,12]. Additionally, the densification temperature of NZTO is much lower than those of other Na-ion conductive oxides such as Na-β/β" alumina [17,18], $Na_3Zr_2Si_2PO_{12}$ [19–21] and $Na_5YSi_4O_{12}$ [22,23].

* Corresponding author.
E-mail address: inada.ryoji.qr@tut.jp (R. Inada).

https://doi.org/10.1016/j.heliyon.2024.e30691
Received 2 March 2024; Received in revised form 29 April 2024; Accepted 2 May 2024
Available online 3 May 2024

In contrast, $Na_2Ni_2TeO_6$ (NNTO) has also been reported as a 3−4 V class cathode active material for rechargeable NiBs with a reversible capacity of 90–100 mAh g^{-1} via the Ni^{2+}/Ni^{3+} and Ni^{3+}/Ni^{4+} redox couples [24–26]. Because of the similarity in their crystal structures and constituent elements, NNTO cathodes and NZTO solid electrolytes can be co-sintered to fabricate oxide based all-solid-state NiBs without undesired side reactions or secondary phase formation at their interface [9]. In this work, we investigated the reactivity between NNTO and NZTO powders co-fired at temperature from 500 to 800 °C. The reaction between NNTO and NZTO is found to be unremarkable at temperature below 700 °C. When co-fired at 800 °C, they form a solid-solution phase with an expected composition of $Na_2Zn_{2-x}Ni_xTeO_6$ (NZNTO). It was found that the solid solution phases of NNTO and NZTO formed at 800 °C show good ionic conducting properties at room temperature.

2. Experimental

2.1. Synthesis of NNTO, NZTO and NNTO-NZTO composites

NNTO and NZTO powders were synthesized by a conventional solid-state reaction method. Na_2CO_3 (Kojundo Chemical Laboratory, 99.5 %), NiO (Kojundo Chemical Laboratory, 99.99 %), ZnO (Kishida Chemical, 99.99 %) and Te_2O_3 (Kojundo Chemical Laboratory, 99.9 %) weighed with the molar ratio of Na: Ni or Zn: Te = 2.2 : 2: 1 (10 % excess Na composition) were mixed and ground with ethanol for 3 h by planetary ball-milling (Nagao System, Planet M2-3F) with zirconia balls with a diameter of 10 mm. The resulting mixture was dried at 80 °C and calcined in an SiC crucible at 850 °C for 6 h in air. The as-prepared NNTO and NZTO powders were mixed in various ratios, ground in an agate mortar and pelletized by cold isostatic pressing at 300 MPa. Mixed NNTO and NZTO pellets were co-fired at 500, 600, 700 and 800 °C for 6 h in air to investigate the reactivity among them.

2.2. Characterization of NNTO, NZTO and NNTO-NZTO composites

The crystal phases of NNTO, NZTO and mixed and co-fired NNTO and NZTO powders were identified by X-ray diffractometer (XRD; Rigaku MultiFlex) using Cu Kα radiation (λ = 0.15418 nm), with a measurement range 2θ of 5–90° and a step interval of 0.002°. Based on the measured XRD data, the lattice constants for *a*-axis and *c*-axis of the as-prepared NNTO or NZTO and co-fired NNTO and NZTO

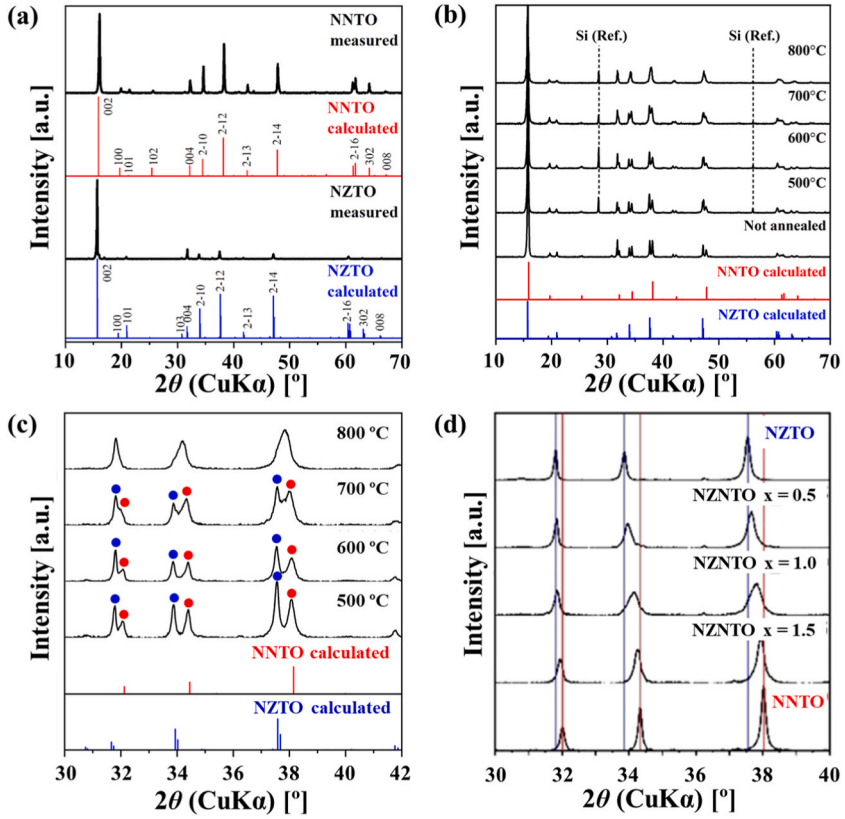

Fig. 1. XRD patterns for (a) calcined NNTO and NZTO powders, (b) and (c) mixed NNTO and NZTO powders (mixing ratio NNTO: NZTO = 1 : 1) after co-firing at 500−800 °C, and (d) mixed powders after co-firing at 800 °C with the different Ni contents x in NZNTO phase. For the measurements, Si was mixed with all samples as the reference material.

powders were calculated using the Rigaku PDXL software [27]. The density of each pelletized sample was estimated by its mass and geometry. The theoretical density for NZTO-NNTO composite pellets were estimated from the theoretical densities NZTO and NNTO, which are 4.88 g cm^{-3} [10] and 4.90 g cm^{-3} [24–26], respectively, and their fraction in the NZTO-NNTO composite pellets. The microstructures of the fractured cross-sectional surfaces of the pelletized NNTO, NZTO and NNTO-NZTO composites with different mixing ratios were observed using field-emission scanning electron microscopy (FE-SEM, SU8000 Type II, Hitachi). The distribution of the constituent elements in the pelletized samples was investigated via energy dispersive X-ray analysis, using FE-SEM.

The ionic conducting properties of all pelletized samples were evaluated using electrochemical impedance spectroscopy. Complex impedance measurement was carried out at room temperature (=27 °C) with an impedance meter (HIOKI IM3536) in a frequency range from 4 Hz to 8 MHz and applied voltage amplitude of 0.01 V. Before the measurements, both parallel end surfaces of each pelletized sample were polished and sputtered with Au films to serve as ion-blocking electrodes. The ionic conductivity of each sample was calculated using geometrical parameters, and the bulk and total (bulk + grain-boundary) resistances were estimated from the impedance data.

3. Results

3.1. Structural analysis of NNTO, NZTO and NNTO-NZTO composites

The XRD patterns of calcined NNTO and NZTO powders are shown in Fig. 1(a). For reference, calculated patterns for NNTO and NZTO based on their structural data were also plotted [10,11]. The peak patterns for both powder samples agreed well with the calculated patterns. The slight difference in the peak patterns between NNTO and NZTO is attributed to the differences in their crystal structures, such as the lattice constants, slab stacking composed of TeO_6 and NiO_6 or ZnO_6 octahedra along the *c*-axis, and interlayer Na distributions [10]. Fig. 1(b) and (c) shows the XRD patterns for mixed NNTO and NZTO powders (mixing molar ratio = 1:1) co-fired at temperatures from 500 to 800 °C. For the measurements, Si was mixed with all samples as a reference material. As shown in Fig. 1(b), no peaks corresponding to the secondary phases were observed. The separation of the diffraction peaks of NNTO and NZTO phases can be confirmed in samples co-fired at 500−700 °C. When co-fired at 800 °C, it became difficult to distinguish the peaks of NNTO and NZTO (Fig. 1(c)), suggesting the formation of a solid-solution phase NZNTO (with Ni content x = 1) [10]. Fig. 1(d) shows the XRD patterns for mixed NNTO and NZTO powders with different mixing molar ratios after co-firing at 800 °C. A monotonous shift in the diffraction peaks with the mixing ratio was confirmed, indicating that the lattice constants of the NZNTO solid solution phases depended on the mixing ratios of NNTO and NZTO (Fig. S1 in the Supplementary Data) [10].

Next, for further investigation, NNTO, NZTO and NNTO-NZTO composite pellets were prepared at 700 and 800 °C for further investigation. As shown in Fig. 2, all the pelletized samples were composed of the grains with the size ranging from 0.5 to 2 μm. Relative densities of each sample calculated from the measured density reduced by the theoretical one, are ranged from 80 to 85 % (Fig. S2 in the Supplementary Data). Although NZNTO solid solution phases were formed in the composite pellets prepared at 800 °C, their theoretical densities are changed slightly from 4.88 to 4.90 g cm^{-3} and gradually increased with increasing Ni content. The difference in the relative density among the samples was unremarkable, however, NNTO showed a slightly lower density than the other samples. Fig. 3 shows SEM images of the NNTO-NZTO composite pellets and the contour mapping of Ni and Zn in the observed areas. In the composite pellets prepared at 700 °C (Fig. 3(a)), Zn and Ni were distributed at different positions in the observed areas. This indicates the insufficient formation of the NZNTO solid-solution phase. On the other hand, it can be confirmed that the distribution of Zn and Ni is more uniform in the composite pellets prepared at 800 °C (Fig. 3(b)), suggesting the promotion of NZNTO phase formation, which was also confirmed by the XRD measurement results (Fig. 1).

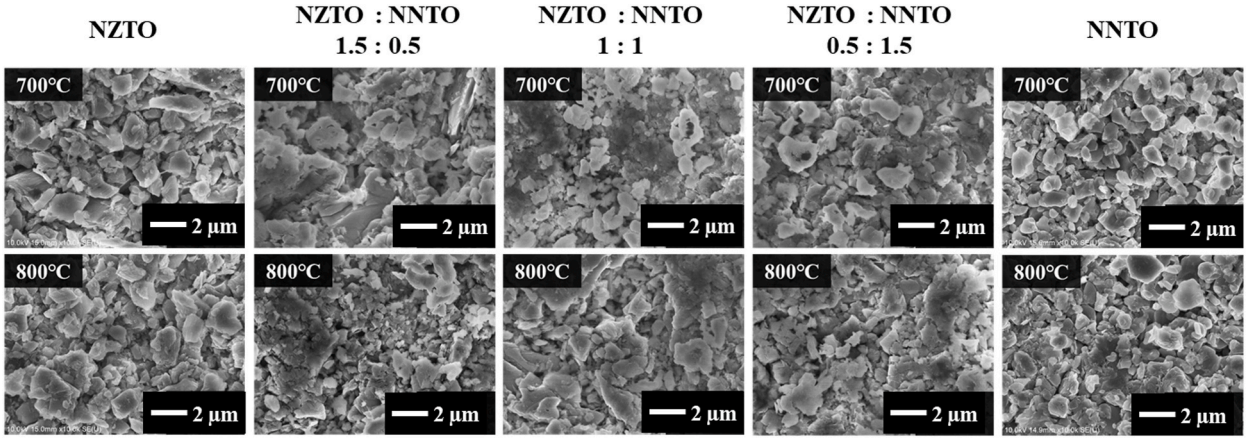

Fig. 2. SEM images for NNTO, NZTO and NZTO-NNTO composite pellets with different mixing ratios prepared at 700 °C (top) and 800 °C (bottom).

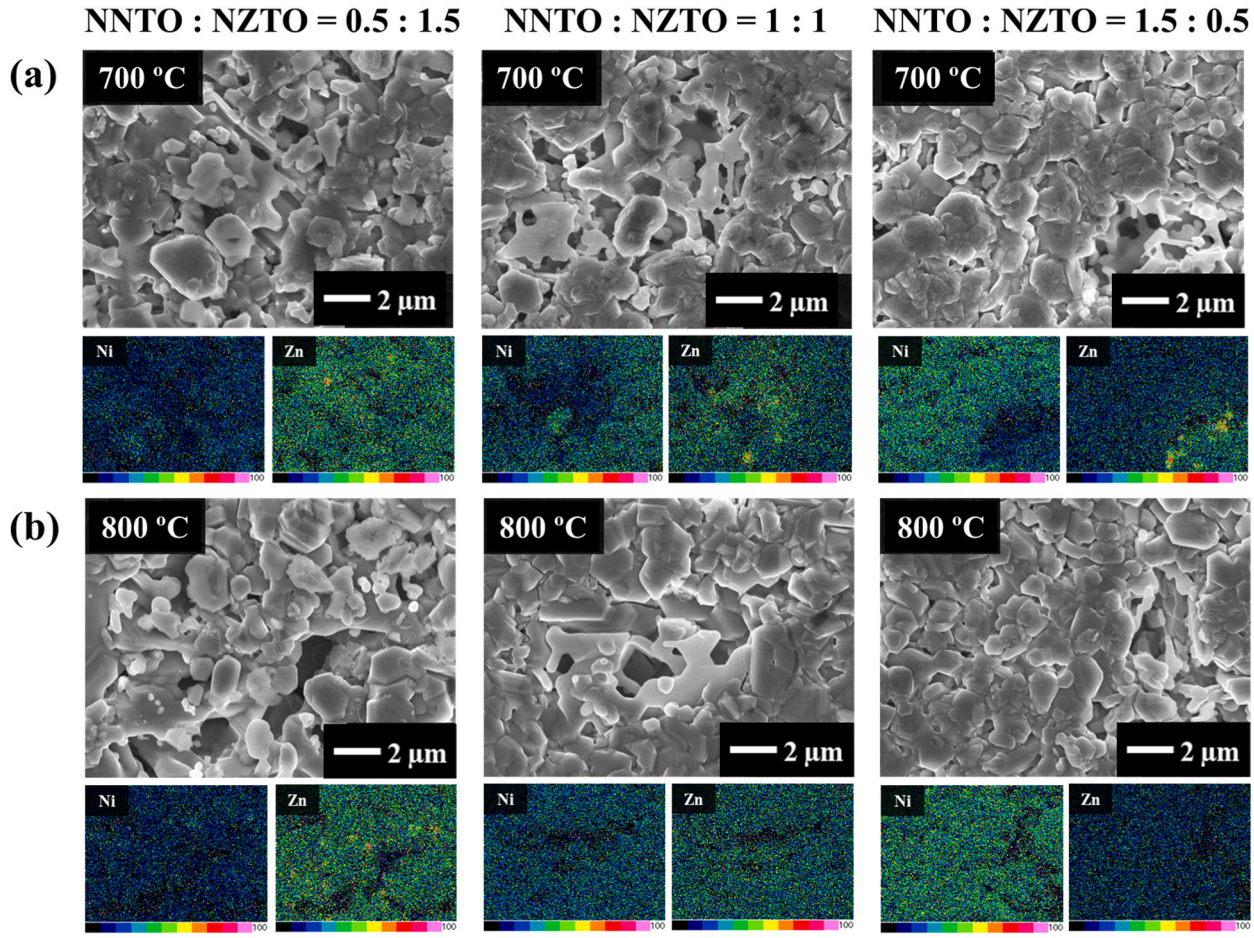

Fig. 3. SEM images and contour maps for Ni and Zn distributions in the observation areas of NNTO-NZTO composite pellets prepared at (a) 700 °C and (b) 800 °C.

3.2. EIS measurement and ionic conductivity of NNTO, NZTO and NNTO-NZTO composites

Fig. 4(a) shows the Nyquist plots of the complex impedance ($Z' + jZ''$) at room temperature for NNTO and NZTO composite pellets co-fired at 800 °C. The real and imaginary parts of complex impedances Z' and Z'', multiplied by a factor of S/t, are plotted for direct comparison of the data for all samples, where S and t are the surface area and thickness of each sample, respectively. The plots are composed of two distorted semicircles at high frequencies and a linear tail in the low frequency range. These data correspond to the ionic conduction at the bulk and grain boundaries and the response of the ionic blocking electrodes, respectively [28]. The dashed lines in Fig. 4(a) represent the fitting curve for the equivalent circuit to the distorted semicircle parts in the plot, consisting of (R_0), (R_1−Q_1), and (R_2−Q_2), where R_0, R_1, R_2, Q_1 and Q_2 correspond to the resistance in the measurement circuit, bulk resistance, grain-boundary resistance, and constant phase angle element (CPE) of the bulk and grain-boundaries. Using R_1 and R_2 values estimated by fitting, the bulk and total (bulk + grain-boundary) ionic conductivities were calculated and summarized in Table 1.

As shown in Fig. 4(b), bulk conductivity reduces gradually with increasing Ni content x in the composite pellet, while total conductivity shows the maximum (=7.4 × 10^{-4} mS cm^{-1}) at x = 0.5 (corresponding to the composition of $Na_2Zn_{1.5}Ni_{0.5}TeO_6$). All composite pellets prepared at 800 °C showed the total conductivity well above 10^{-4} S cm^{-1} at room temperature, which are superior to NZTO (=3.8 × 10^{-4} mS cm^{-1}) and NNTO (=2.5 × 10^{-4} mS cm^{-1}) pellets prepared at the same condition. These results can be applied to form a solid-solid interface in all-solid-state NiBs with NNTO as the cathode and NZTO as the solid electrolyte via a simple co-sintering process.

4. Discussion

To determine why bulk conductivity and total conductivity show different Ni content dependences, Fig. 4(c) shows the contribution of grain-boundary resistance to the total (bulk + grain-boundary) one for NNTO-NZTO composite pellets prepared at 800 °C. Compared to NZTO, NNTO-NZTO composites have lower contribution of grain-boundary resistance, indicating that the formation of

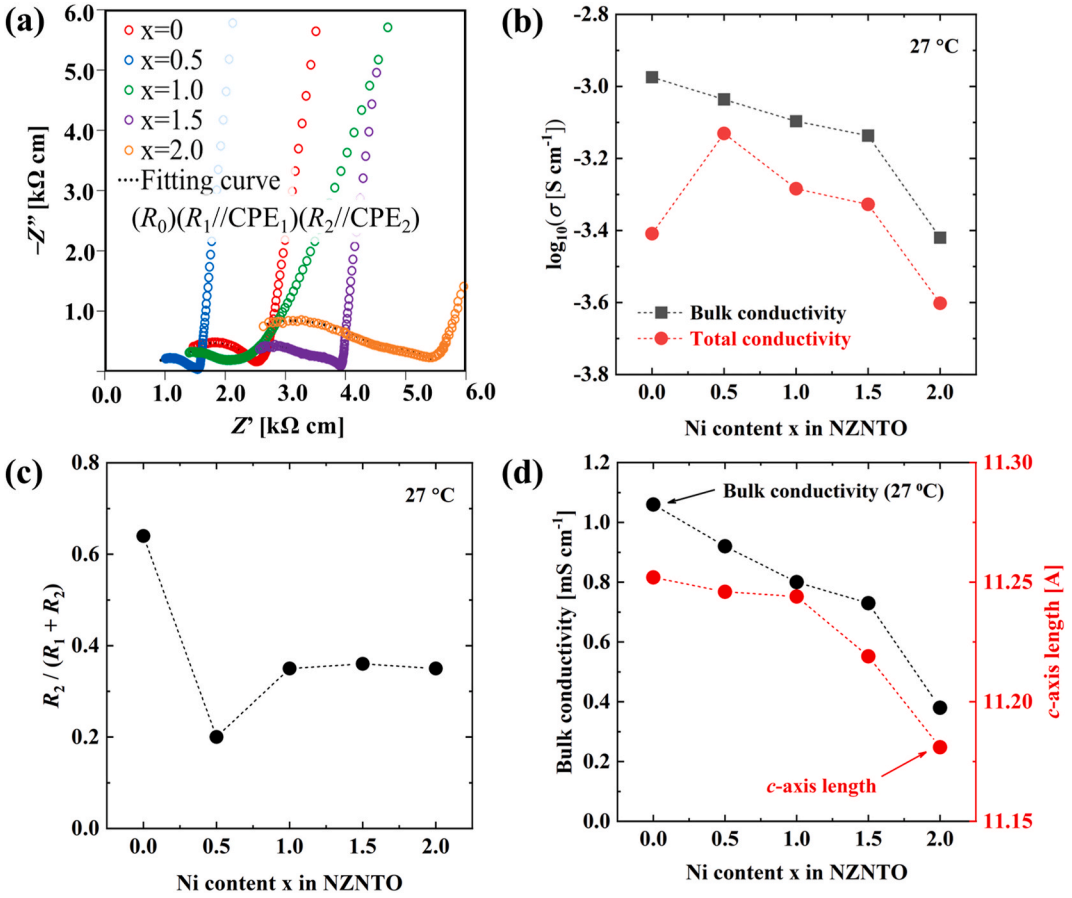

Fig. 4. (a) Nyquist plots for complex impedance at room temperature, (b) Room temperature bulk and total (bulk + grain-boundary) conductivity, (c) fraction of grain-boundary resistance R_2 in total resistance $R_1 + R_2$ for NZNTO pellets with different Ni content x prepared at 800 °C, and (d) bulk conductivity and *c*-axis length for NZNTO with different Ni content x prepared at 800 °C.

Table 1
Bulk resistivity R_1, grain-boundary resistivity R_2, bulk and total ionic conductivity of pelletized NNTO, NZTO and NNTO-NZTO composites prepared at 800 °C. The fractions of R_2 in total resistivity ($R_1 + R_2$) are also shown in the table.

Sample	R_1 [Ω cm]	R_2 [Ω cm]	$R_2/(R_1 + R_2)$	Ionic conductivity [mS cm^{-1}]	
				Bulk	Total
NZTO	945	1658	0.64	1.06	0.38
NNTO-NZTO (0.5 : 1.5)	1087	264	0.20	0.92	0.74
NNTO-NZTO (1 : 1)	1243	670	0.35	0.80	0.52
NNTO-NZTO (1.5 : 0.5)	1379	763	0.36	0.73	0.47
NNTO	2608	1402	0.35	0.38	0.25

the NZNTO phase has a positive effect on reducing the grain boundary resistance. During the co-firing of NZTO and NNTO at 800 °C, NZNTO phase is formed through the mutual diffusion of Ni in NNTO grains and Zn in NZTO grains. It is speculated that this contributes to increasing the intergranular connectivity and lowering the grain-boundary resistance. Although the difference in compositional dependencies of bulk and total conductivity are related to the degree of contribution of grain boundary resistance, the reason why the grain boundary resistance is mitigated at a Ni content of 0.5 is not well clarified. Therefore, a more detailed investigation is required.

As reported in literature [29,30], the Na-ion conductivity of P2-type honeycomb layered oxide strongly depends on the interlayer spacing along the *c*-axis. In Fig. 4(d), the bulk conductivity and *c*-axis length for all samples sintered at 800 °C are plotted against the Ni content in the NZNTO solid-solution phase. It is evident that bulk conductivity tends to decrease with increasing Ni contents and decreasing *c*-axis length. NZTO has a much higher bulk conductivity (=1.06×10^{-3} S cm^{-1}) than NNTO (=3.8×10^{-4} S cm^{-1}). Smaller interlayer spacing along *c*-axis increases the attractive force between Na^+ and O_2^-, resulting in a larger migration energy of Na^+ and lower bulk ionic conductivity.

Lastly, it is worth noting that the total conductivity of pelletized samples prepared at 700 °C was lower than the samples prepared at

800 °C (Fig. S3 in the Supplementary Data), probably owing to poor sintering and/or insufficient formation of the solid solution phase. A higher processing temperature may further improve the total conductivity; however, sodium volatilization must be considered [14, 15]. Moreover, a lower co-firing temperature may be preferable for preserving the function of NNTO as a cathode and the electrochemical stability of NZTO as a solid electrolyte. Because the densification temperature of NZTO can be reduced to 700 °C or less by applying hot pressing (HP) [17], we believe that a highly conductive solid-solid interface between NNTO and NZTO in the composite can be formed by tuning the co-firing temperature in HP.

5. Conclusion

The reactivity of NNTO and NZTO co-fired at temperatures from 500 °C to 800 °C was systematically invesitigated. It was found that the reaction between NNTO and NZTO is not remarkable at co-firing temperature below 700 °C. However, when annealed at 800 °C, they formed the NZNTO solid-solution phase without forming any secondary phases. NNTO and NZTO composite pellets co-fired at 800 °C showed total ionic conductivity well above 10^{-4} S cm^{-1} at room temperature, indicating that the NZNTO phase has good ionic conducting property. The obtained results provide fundamental information for the fabrication of all-solid-state battery with NNTO as the cathode and NZTO as the solid electrolyte via co-sintering.

Data availability statement

Data associated with our study have not been deposited into a publicly available repository but will be made available on request.

CRediT authorship contribution statement

Kazuki Yamamoto: Writing – original draft, Visualization, Investigation, Formal analysis, Data curation, Conceptualization. **Yuki Ono:** Writing – original draft, Methodology, Investigation, Formal analysis, Data curation. **Ryoji Inada:** Writing – review & editing, Writing – original draft, Visualization, Validation, Supervision, Resources, Project administration, Methodology, Investigation, Funding acquisition, Formal analysis, Data curation, Conceptualization.

Declaration of competing interest

The authors declare that they have no competing financial interests or personal relationships that could have appeared to influence the work reported in this paper.

Acknowledgements

This work was partly supported by Grant-in-Aid for Scientific Research (JSPS KAKENHI) Grant Number 23K22739 from the Japan Society for the Promotion of Science (JSPS) and the Foundation of Public Interest of Tatematsu, Japan. We would like to thank Editage (https://www.editage.jp/) for English language editing, and acknowledge the support of the Cooperative Research Facility Center at Toyohashi University of Technology.

Appendix A. Supplementary data

Supplementary data to this article can be found online at https://doi.org/10.1016/j.heliyon.2024.e30691.

References

[1] A. Rudola, C.J. Wright, J. Barker, Reviewing the safe shipping of lithium-ion and sodium-ion cells: a materials chemistry perspective, Energy Mater. Adv. 2021 (2021) 9798460.
[2] W. Zhou, Y. Li, S. Xin, J.B. Goodenough, Rechargeable sodium all-solid-state battery, ACS Cent. Sci. 3 (2017) 52–57.
[3] W. Hou, X. Guo, X. Shen, K. Amine, H. Yu, J. Lu, Solid electrolytes and interfaces in all-solid-state sodium batteries: Progress and perspective, Nano Energy 52 (2018) 279–291.
[4] C. Zhou, S. Bag, V. Thangadurai, Engineering materials for progressive all-solid-state Na batteries, ACS Energy Lett. 3 (2018) 2181–2198.
[5] C. Chao, L. Liu, X. Qi, Y. Lu, F. Wu, J. Zhao, Y. Yu, Y.S.Y.S. Hu, L. Chen, Solid-state sodium batteries, Adv. Energy Mater. 8 (2018) 1703012.
[6] Q. Ma, F. Tietz, Solid-state electrolyte materials for sodium batteries: towards practical applications, Chemelectrochem 7 (2020) 2693–2713.
[7] G. Liu, J. Yang, J. Wu, Z. Peng, X. Yao, Inorganic sodium solid electrolytes: structure design, interface engineering and application, Adv. Mater. (2024) 2311475.
[8] M.A. Evstigneeva, V.B. Nalbandyan, A.A. Petrenko, B.S. Medvedev, A.A. Kataev, A new family of fast sodium ion conductors: $Na_2M_2TeO_6$ (M = Ni, Co, Zn, Mg), Chem. Mater. 23 (2011) 1174–1181.
[9] R. Berthelot, W. Schmidt, A.W. Sleight, M.A. Subramanian, Studies on solid solutions based on layered honeycomb-ordered phases P2-$Na_2M_2TeO_6$ (M=Co, Ni, Zn), J. Solid State Chem. 196 (2012) 225–231.
[10] Y. Li, Z. Deng, J. Peng, E. Chen, Y. Yu, X. Li, J. Luo, Y.-Y. Huang, J. Zhu, C. Fang, Q. Li, J. Han, A P2-type layered superionic conductor Ga-doped $Na_2Zn_2TeO_6$ for all-solid-state sodium-ion batteries, Chem. Eur J. 24 (2018) 1057–1061.
[11] J.-F. Wu, Q. Wang, X. Guo, Sodium-ion conduction in $Na_2Zn_2TeO_6$ solid electrolytes, J. Power Sources 402 (2018) 513–518.
[12] Z. Deng, J. Gu, Y. Li, S. Li, J. Peng, X. Li, J. Luo, Y.-Y. Huang, C. Fang, Q. Li, J. Han, Y. Huang, Y. Zhao, Ca-doped $Na_2Zn_2TeO_6$ layered sodium conductor for all-solid-state sodium-ion batteries, Electrochim. Acta 298 (2019) 121–126.

[13] X. Li, F. Bianchini, J. Wind, C. Pettersen, D.S. Wragg, P. Vajeeston, H. Fjellvag, Insights into crystal structure and diffusion of biphasic $Na_2Zn_2TeO_6$, ACS Appl Mater Interfaces ACS Appl. Mater. Interfaces 12 (2020) 28188–28198.
[14] A. Itaya, K. Yamamoto, R. Inada, Y. Sakurai, Effect of excess Na contents in precursor on the property of $Na_2Zn_2TeO_6$ ceramic solid electrolyte, Mater. Lett. 284 (2021) 128941.
[15] A. Itaya, K. Yamamoto, R. Inada, Sintering temperature dependency on sodium-ion conductivity for $Na_2Zn_2TeO_6$ solid electrolyte, Int. J. Appl. Ceram. Technol. 18 (2021) 2085–2090.
[16] A. Itaya, Y. Ono, K. Yamamoto, R. Inada, Characterization of $Na_2Zn_2TeO_6$ ceramic solid electrolyte densified by hot pressing, Int. J. Appl. Ceram. Technol. 21 (2024) 311–318.
[17] G.E. Youngblood, G.R. Miller, R.S. Gordon, Relative effects of phase conversion and grain size on sodium ion conduction in polycrystalline, lithia-stabilized β-alumina, J. Am. Ceram. Soc. 61 (1978) 86–87.
[18] X. Lu, G. Xia, J.P. Lemmon, Z. Yang, Advanced materials for sodium-beta alumina batteries: Status, challenges and perspectives, J. Power Sources 195 (2010) 2431–2442.
[19] J.B. Goodenough, H.Y.-P. Hong, J.A. Kafalas, Fast Na^+-ion transport in skeleton structure, Mater. Res. Bull. 11 (1976) 203–220.
[20] Q. Ma, C.-L. Tsai, X.-K. Wei, M. Heggen, F. Tietz, J.T.S. Irvine, Room temperature demonstration of a sodium superionic conductor with grain conductivity in excess of 0.01 S cm^{-1} and its primary applications in symmetric battery cells, J. Mater. Chem. A 7 (2019) 7766–7776.
[21] Q. Zhang, Y. Lu, W. Guo, Y. Shao, L. Liu, J. Lu, X. Rong, X. Han, H. Li, L. Chen, Y.-S. Hu, Hunting sodium dendrites in NASICON-based solid-state electrolytes, Energy Mater. Adv. 2021 (2021) 9870879.
[22] G. Sun, X. Yang, N. Chen, S. Yao, X. Wang, X. Jin, G. Chen, Y. Xie, F. Du, $Na_5YSi_4O_{12}$: a sodium superionic conductor for ultrastable quasi-solid-state sodium-ion batteries, Energy Storage Mater. 41 (2021) 196–202.
[23] A. Sivakumaran, A.J. Samson, V. Thangadurai, Progress in sodium silicates for all-solid-state sodium batteries—a review, Energy Technol. 11 (2023) 2201323.
[24] A. Gupta, C.B. Mullins, J.B. Goodenough, $Na_2Ni_2TeO_6$: Evaluation as a cathode for sodium battery, J. Power Sources 243 (2013) 817–821.
[25] T. Masese, Y. Miyazaki, J. Rizell, G.M. Kanyolo, T. Takahashi, N. Ito, H. Senoh, T. Saito, Unveiling structural disorders in honeycomb layered oxide: $Na_2Ni_2TeO_6$, Materialia 15 (2021) 101003.
[26] W. Wang, J. Zhang, C. Li, X. Kou, B. Li, D.Y.W. Yu, P2-$Na_{2/3}Ni_{2/3}Te_{1/3}O_2$ cathode for Na-ion batteries with high voltage and excellent stability, Energy Environ. Mater. 6 (2023) e12314.
[27] PDXL: Integrated X-ray powder diffraction software - Rigaku, https://www.rigaku.com/support/software/pdxl..
[28] K. Akimoto, Y. Sugimura, R. Inada, Characterization of garnet-type $Li_6SrLa_2Bi_2O_{12}$ ceramic electrolyte for all-solid-state Li-ion batteries, Mater. Lett. 349 (2023) 134866.
[29] Y. Li, Z. Deng, J. Peng, J. Gu, E. Chen, Y. Yu, J. Wu, X. Li, J. Luo, Y. Huang, Y. Xu, Z. Gao, C. Fang, J. Zhu, Q. Li, J. Tan, Y. Huang, New P2-type honeycomb-layered sodium-ion conductor: $Na_2Mg_2TeO_6$, ACS Appl. Mater. Interfaces 10 (2018) 15760–15766.
[30] H. Huang, Y. Yang, C. Cheng, H.-H. Wu, B. Huang, Phase stability and fast ion transport in P2-type layered $Na_2X_2TeO_6$ (X = Mg, Zn) solid electrolytes for sodium batteries, J. Mater. Chem. A. 8 (2020) 22816–22827.